JCB

Supplemental material

Xia et al., https://doi.org/10.1083/jcb.201811100

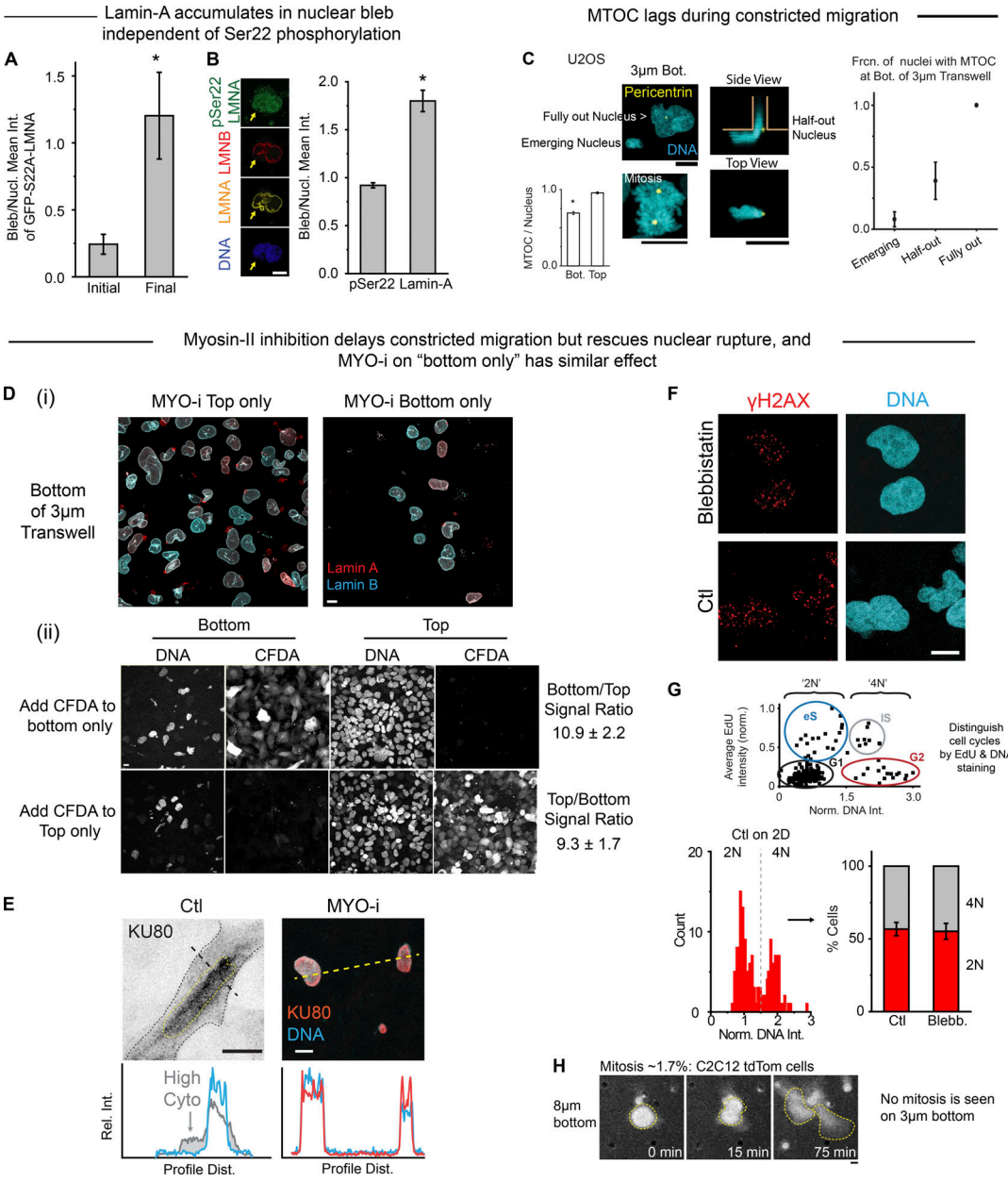

Figure S1. **Phospho-lamin-A, MTOC, and myosin II effects in and on constricted migration and/or rupture. (A)** GFP-S22A-LMNA accumulates in nuclear blebs over time, causing the bleb-to-nucleus GFP intensity ratio to increase after bleb formation (n = 3 cells; *, P < 0.05). Nucl. Int., nuclear intensity. **(B)** Immunostaining of nuclei on the bottom (Bot.) of a 3-µm pore filter indicates enrichment of lamin-A but not lamin-B or pSer22-lamin-A in nuclear blebs (n > 5 cells; *, P < 0.05). **(C)** MTOC staining (pericentrin) is confirmed in mitotic cells. Some nuclei on the bottom of a 3-µm pore filter do not have visible MTOCs (lower image, yellow arrow), giving bottom a lower MTOC-per-nucleus fraction (Frcn.) than top (bar graph). This lower fraction indicates the MTOC is not typically oriented toward the leading edge of a pore-migrating U2OS nucleus. Hence, in nuclei that are just emerging from pores, MTOCs are not visible on the membrane bottom. As nuclei emerge further, some MTOCs become visible outside the pore (images of Half-out Nucleus). Once the whole nucleus has completely migrated, the MTOC is invariably seen on bottom (right plot, >48 cells per condition, n ≥ 3 experiments; *, P < 0.05). **(Di)** Representative images show U2OS nuclei after migration through 3-µm pores. Blebbistatin (MYO-i) was added either only on top of the 3-µm pore filter (left) or only on bottom (right). **(Dii)** When added only to the top or bottom of a Transwell pore filter, small molecules such as the cell-permeable dye CFDA do not cross to the other side of the filter (⩽10%, n = 3 experiments). **(E)** A representative immunofluorescence image shows a ruptured control (Ctl) nucleus with mislocalization of endogenous KU80 from the nucleus into the cytoplasm. After MYO-i treatment, rupture is rescued, as KU80 does not mislocalize. Dist., distribution; Rel. Int., relative intensity. **(F)** Representative images show DNA and DNA damage in 3-µm pore–migrated cells with and without MYO-i treatment. **(G)** EdU was added to 3- and 8-µm pore membranes for 1 h just before the membranes were formaldehyde-fixed and immunostained; EdU-labeled cells were stained by a "click" chemistry reaction. The average EdU intensity of individual cells, measured by immunofluorescence microscopy, was used to identify cells in the S phase of cell cycle, while total DNA intensity distinguished nonreplicated (2N) genomes from twice-as-large, fully replicated (4N) genomes. In this way, all cells on the top and bottom of the Transwell membranes were classified as G1, early S (eS), late S (lS), or G2. Intensities are normalized (Norm.) to maximum values. In 2D culture, 2N and 4N cells can be clearly separated based on the valley between two DNA peaks. Blebbistatin (Blebb.) does not affect cell cycle, as 2N and 4N populations stay the same in control and MYO-i groups after 24-h treatment (n = 3 experiments). **(H)** Dashed line outlines a representative mitotic C2C12 cell with integrated tdTomato (tdTom) signal on bottom of 8-µm Transwell. All scale bars: 10 µm.

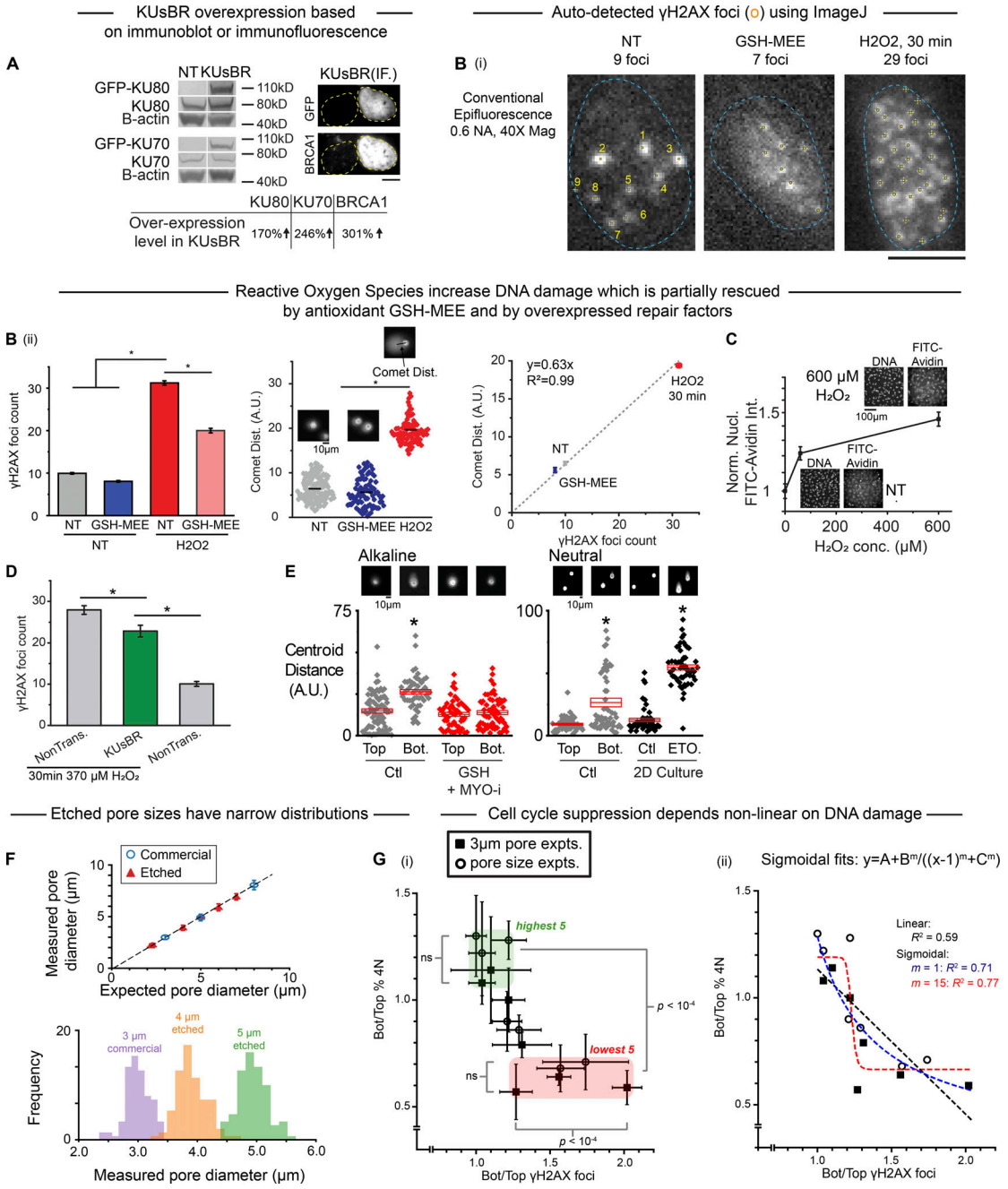

Figure S2. **Repair factors, reactive oxygen species, and MYO-i effects on DNA damage and cell cycle, including use of etched pores for migration. (A)** Quantification of overexpression level by either Western blot or immunofluorescence (IF; *n* = 3 experiments). **(B)** H_2O_2 (370 µM, 30 min) severely damages DNA. **(Bi)** Yellow dots are foci recognized automatically by ImageJ algorithm and labeled. Mag, magnification. **(Bii)** DNA fragments are detected by electrophoretic comet assays: nuclei isolated after H_2O_2 treatment show more of a cathode-shifted centroid of DNA with a higher mean displacement (inset images) compared with nuclei isolated from non-treated (NT) and GSH-MEE groups (50–100 cells per condition, *n* = 3 experiments; *, P < 0.05). DNA damage measured in parallel for γH2AX foci and comet distance shows a linear correlation. The excess damage can be partially rescued by adding 1 mg/ml GSH-MEE (200–700 cells per group, *n* > 3 experiments; * P < 0.05). Scale bar: 10 µm. A.U., arbitrary units; Dist., distance. **(C)** FITC-labeled avidin has a high specific affinity for 8-oxoguanine, an oxidized base in DNA. Half-hour incubation with 60 or 600 µM H_2O_2 results in elevated nuclear FITC-avidin signal, suggesting increased oxidative stress (>120 cells per group; *, P < 0.05; *n* = 2 experiments). conc., concentration; Norm., normalized; Nucl. Int., nuclear intensity. **(D)** Co-overexpression of KUsBR reduces H_2O_2-induced DNA damage, although not to the basal level measured in nontransfected (NonTrans.) cells without H_2O_2 (28–132 cells per condition, *n* = 3 experiments; *, P < 0.05). **(E)** Alkaline comet assay confirms that DNA damage is higher on bottom of 3-µm Transwell, and such damage can be rescued by GSH-MEE+MYO-i. Neutral comet confirms that DNA damage is higher on bottom of 3-µm Transwell. 10 µM Etoposide (ETO) is used as a positive control (Ctl). **(F)** Commercially available (Corning) and custom-etched Transwell membranes were imaged by confocal microscopy, and their pore diameters were measured in ImageJ. For every membrane, the measured pores are highly uniform in size, based on low SD, and match expected diameter values (one Transwell per condition; *n* = 100 pores for the 3-µm commercial and 4- and 5-µm etched membranes; for all other membranes, *n* = 40 pores; error bars give SD). Histograms show tight pore diameter distributions for the 3-µm commercial and 4- and 5-µm etched membranes. **(Gi)** Data points in Fig. 3 E are plotted with error bars. **(Gii)** Linear fit has a low R^2 versus sigmoidal fits. expt., experiments; bot., bottom.

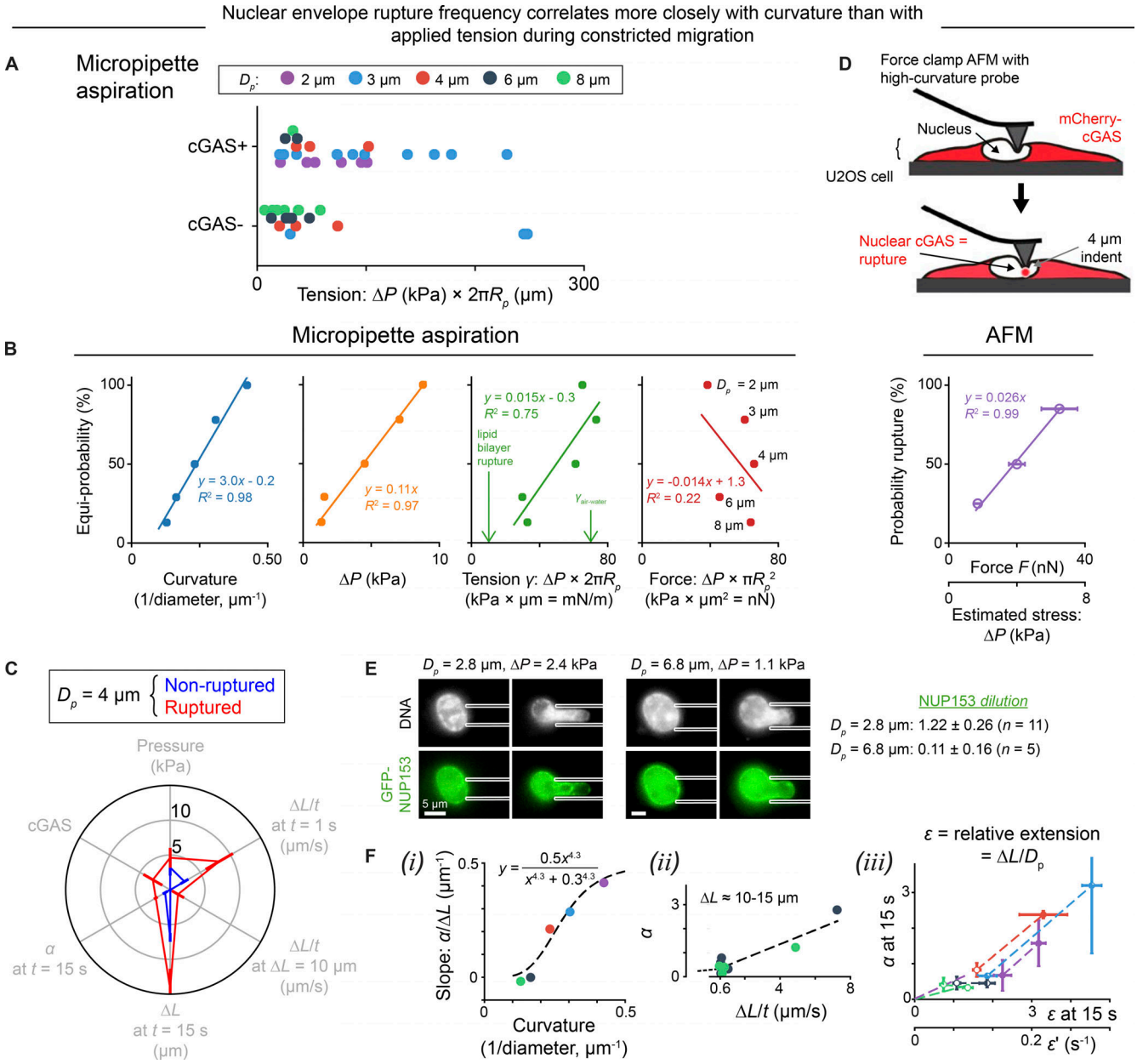

Figure S3. **Nuclear envelope rupture frequency correlates more with curvature and pressure than with applied tension. (A)** After detachment and latrunculin treatment, U2OS cells overexpressing mCherry-cGAS and lamin-B1-GFP were passively pulled into micropipettes of diameter D_p ≈ 2, 3, 4, 6, and 8 µm. Each data point represents a single aspirated cell, which is classified as cGAS-positive (cGAS$^+$) if it exhibits nuclear entry of mCherry-cGAS during aspiration, signifying nuclear envelope rupture. Tension is given by applied pressure (which varied between cells) times pipette circumference (R_p = pipette radius). **(B)** Using the data in panel A, a critical tension T_{crit} was defined for each D_p such that the probability of nuclear envelope rupture is the same for $T < T_{crit}$ and $T > T_{crit}$. Critical pressure and critical force were determined in the same way. Referring to the rupture probability at T_{crit} as the equi-probability, we plot equi-probability as a function of curvature, critical pressure, critical tension, and critical force for every D_p. Equi-probability yields a better fit (higher R^2) when plotted against curvature or against pressure than against tension. **(C)** Spider plot summarizes quantification of detached, latrunculin-treated U2OS cells that either exhibit nuclear envelope rupture (red) or not (blue) when passively pulled into micropipettes of diameter D_p = 4 µm. Each polar axis represents a different measurement. ΔL/t at t = 1 s and at ΔL = 10 µm are reported in Fig. 4 Eii; ΔL and α at t = 15 s are reported in Fig. 4 Ei; and cGAS and pressure are drawn from the datasets in Fig. 4 D and Fig. S3 B, respectively. Explanations of these parameters can be found in the corresponding figure legends (six cells total, three cells per condition; error bars show SEM). **(D)** Probing nuclei in living U2OS cells with high-curvature beads (diameter <0.1 µm) reveals a strong correlation between applied force (or stress) and probability of nuclear envelope rupture, as indicated by nuclear entry of mCherry-cGAS. Importantly, because the probe is of height h = ∼4 µm (schematic diagram), the depth of AFM indentation is low compared with the nuclear extension ΔL achieved in micropipettes (seven cells total, two or more cells per bin; SEM). **(E)** U2OS cells overexpressing GFP-Nup153 show dilution of nuclear pore complex proteins at the leading tip of the nucleus when passively pulled into constricting pipettes (D_p = 2.8 µm) but not larger (D_p = 6.8 µm) pipettes (five or more cells per D_p; scale bar: 5 µm). **(F)** Based on Fig. 4 Ei. **(Fi)** The slope α/ΔL was calculated for each D_p; slope increases with curvature. **(Fii)** Large pipettes (6 and 8 µm) dilute lamin-B1 (high α) only for extremely rapid extension of the nucleus. Data at ΔL/t ≈ 0.6 µm/s are from Fig. 4 Ei; upper points are cells fully aspirated within t ≈ 3 s and were not included in Fig. 4 Ei. **(Fiii)** Fig. 4 Ei is reproduced here, with the parameter ΔL (i.e., the extension of the nucleus into the pipette) replaced by the dimensionless parameter ε, which is ΔL at t ≈ 15 s normalized to pipette diameter D_p. The rate ε′ is defined as ε/t.

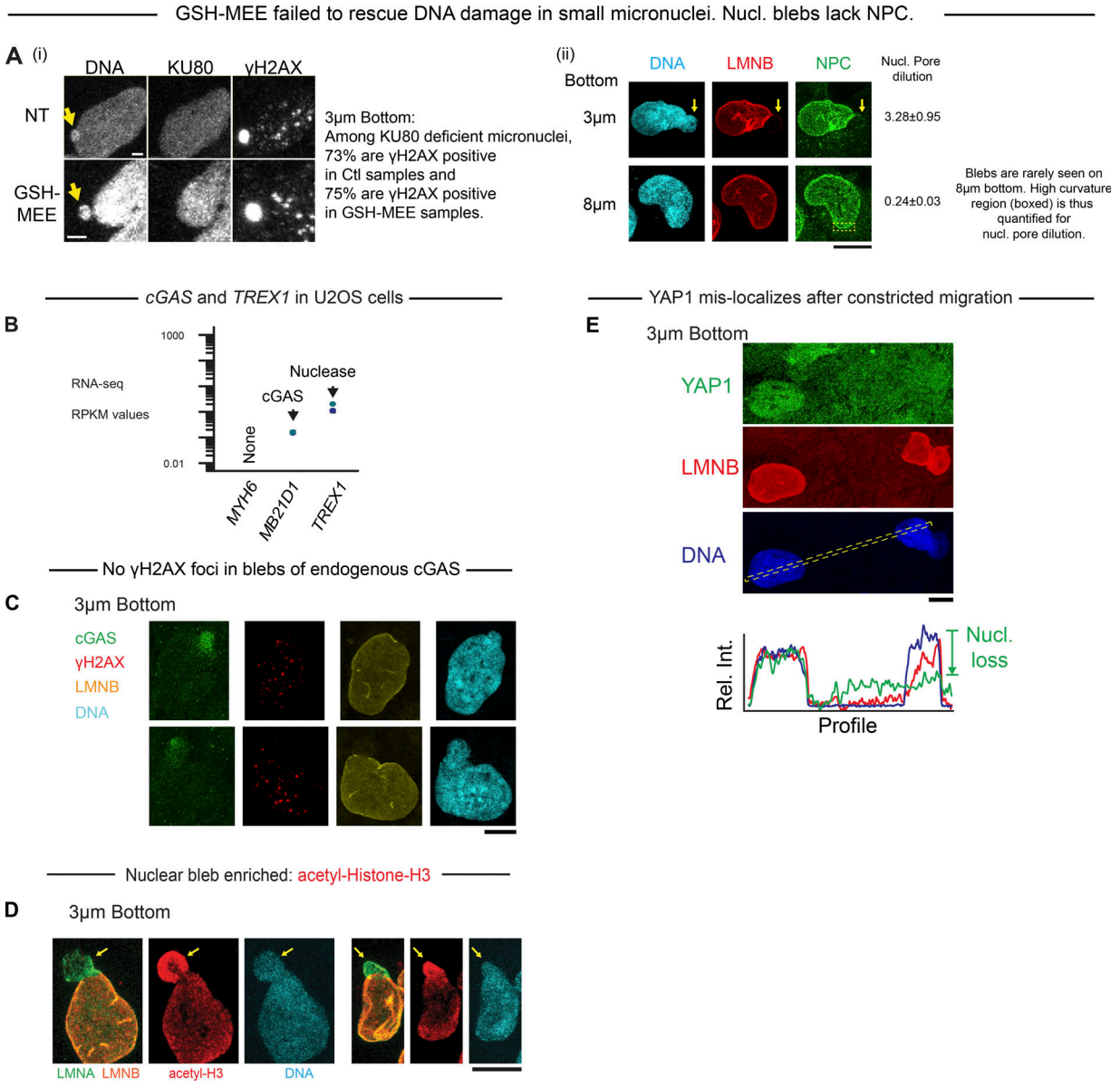

Figure S4. **Composition of micronuclei, nuclear blebs, and ruptured nuclei. (Ai)** GSH-MEE does not reduce the fraction of γH2AX-positive micronuclei (Nucl.) that lack KU80 (n = 10). Scale bar: 2 µm. **(Aii)** Ruptured nuclei are deficient in nuclear pore complexes on the bleb (arrows), similar to lamin-B. The dilution calculation is described in Materials and methods Calculating lamin-B dilution (>10 cells per condition, n = 3 experiments). Scale bar: 10 µm. **(B)** In U2OS cells, RNA-seq data reveals expression of at least two cytoplasmic factors, *TREX1* and *cGAS* (*MB21D1*), which might interact with chromatin after nuclear envelope rupture. RPKM, reads per kilobase of transcript per million mapped reads. **(C)** Endogenous cGAS binds to DNA in nuclear blebs, as seen in representative images of U2OS cells after 3-µm pore migration. DNA damage foci do not localize to blebs, the sites of cGAS accumulation. **(D)** Representative images of 3-µm pore–migrated U2OS cells show that nuclear blebs have abundant acetylated chromatin. **(E)** YAP1 mislocalizes to cytoplasm after nuclear rupture. All scale bars are 10 µm unless stated otherwise. Rel. Int., relative intensity.

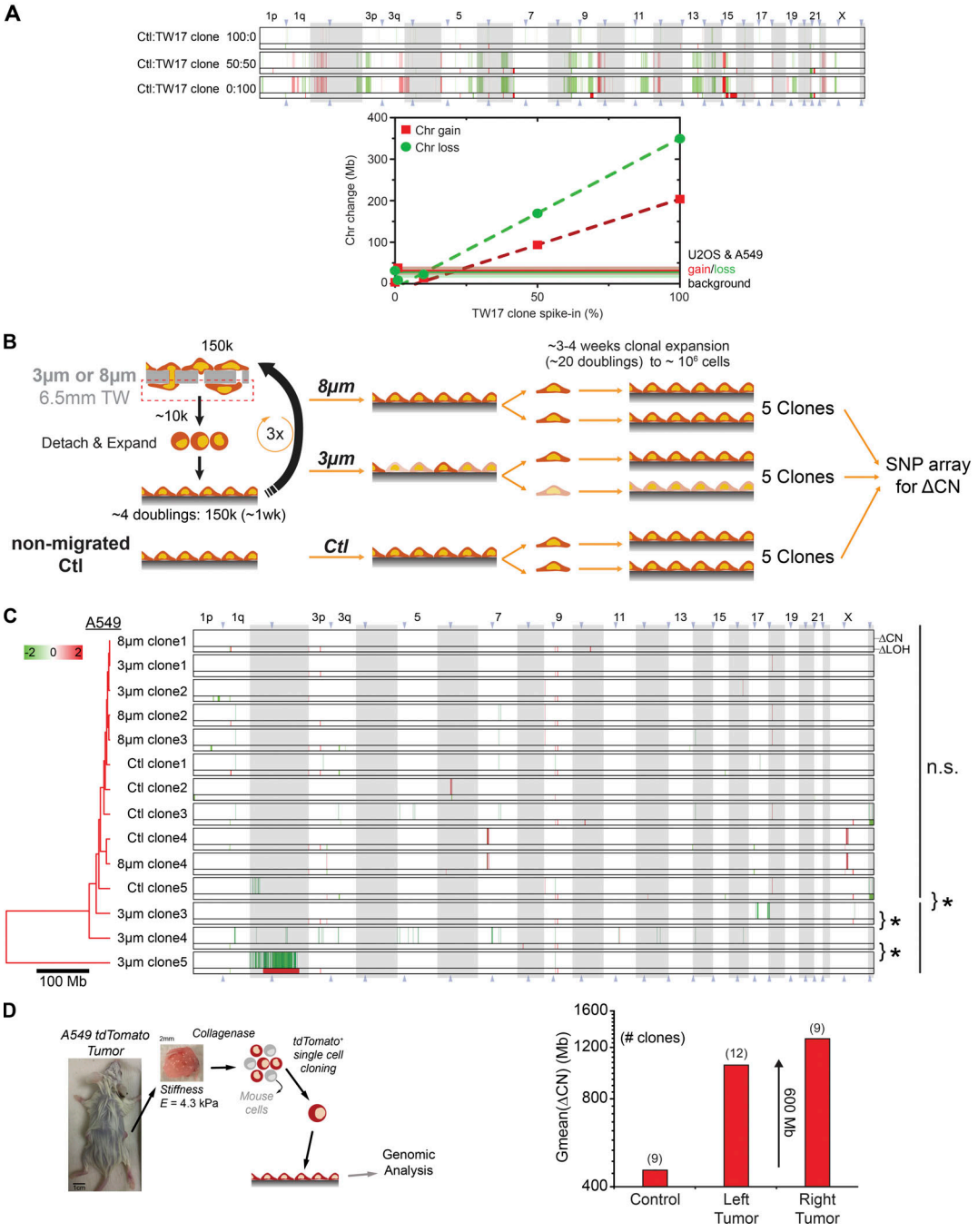

Figure S5. **Genomic variation measurements after constricted migration. (A)** To characterize the uncertainty associated with reproducibility of our SNP array data, we performed three separate SNP arrays with the same sample. The variation is 40 Mb (from the 3,100-Mb array). Additionally, two distinguishable U2OS samples generated in our previous study (Irianto et al., 2017) were mixed and subjected to SNP array analysis. The real signal for genomic variation becomes linear and detectable at chromosome (Chr) change >40 Mb (see Materials and methods, Genome (SNP array) analysis, for details). Ctl, control. **(B)** Schematics: A549 cells were subjected to three rounds of Transwell migration through 3- or 8-µm pores to test the hypothesis that at least some DNA damage would be survivable but misrepaired. Nonmigrated control clones were expanded in parallel. From among these thrice-migrated or nonmigrated cells, the genomes of multiple single cell–derived clones were quantified by SNP array analysis. Time span and doublings for each step are indicated. **(C)** Compared with a clone that migrated three times through 8-µm pores, significant chromosome copy number changes (ΔCN) and loss of heterozygosity (ΔLOH) above the noise level (40 Mb) are observed in three of five A549 clones that migrated through 3-µm pores. Clones are listed per hierarchical clustering of their ΔCN, and the asterisk indicates statistical significance in the overall distribution of gains (red) and losses (green); *, $P < 0.05$ in Kolmogorov-Smirnov test; see Materials and methods, Genome (SNP array) analysis for details). n.s., not significant. **(D)** Schematic: A549 tdTomato cells were injected subcutaneously into the left and right flanks of nonobese diabetic/severe combined immunodeficient mice ($n \geq 3$ mice). After 4 wk, tumors were harvested and disaggregated, and SNP array analysis was performed on single cell–derived tdTomato$^+$ clones. Bar graph: Clones from both the left and right tumors exhibited significant ΔCN compared with control cells cultured on 2D plastic. This increase in genomic variation is similar in magnitude to that observed after constricted migration.

References

Irianto, J., Y. Xia, C.R. Pfeifer, A. Athirasala, J. Ji, C. Alvey, M. Tewari, R.R. Bennett, S.M. Harding, A.J. Liu, et al. 2017. DNA Damage Follows Repair Factor Depletion and Portends Genome Variation in Cancer Cells after Pore Migration. *Curr. Biol.* 27:210–223. https://doi.org/10.1016/j.cub.2016.11.049